1988ApJ...324.1106B

THE ASTROPHYSICAL JOURNAL, 324:1106–1117, 1988 January 15
© 1988. The American Astronomical Society. All rights reserved. Printed in U.S.A.

COSMIC-RAY ENERGY SPECTRA BETWEEN 10 AND SEVERAL HUNDRED GeV PER ATOMIC MASS UNIT FOR ELEMENTS FROM $_{18}$Ar TO $_{28}$Ni: RESULTS FROM *HEAO 3*

W. R. BINNS,[1] T. L. GARRARD,[2] M. H. ISRAEL,[1] MICHAEL D. JONES,[1] M. P. KAMIONKOWSKI,[1] J. KLARMANN,[1] E. C. STONE,[2] AND C. J. WADDINGTON[3]

Received 1987 May 8; accepted 1987 July 13

ABSTRACT

The Heavy Nuclei Experiment on *HEAO 3* included ionization chambers and a Cherenkov detector. For nuclei that arrive at locations and from directions with high geomagnetic cutoff (>8 GV) the Cherenkov signal determines the atomic number, Z, while the relativistic rise in ionization provides a measure of the energy. For the secondary cosmic-ray elements, $_{19}$K, $_{21}$Sc, $_{22}$Ti, and $_{23}$V, the abundances relative to $_{26}$Fe fall as power laws in energy; combining our results from 10 to ~200 GeV per amu with data between 1 and 25 GeV per amu from another instrument on the same spacecraft gives exponents -0.31 ± 0.01, -0.25 ± 0.02, -0.28 ± 0.01, and -0.23 ± 0.02, respectively. For $_{28}$Ni, which like $_{26}$Fe is a primary element, the abundance relative to $_{26}$Fe is essentially independent of energy over the interval from ~10–500 GeV per amu. The elements $_{18}$Ar and $_{20}$Ca, which at a few GeV per amu are mixtures of primary and secondary components, display abundances relative to $_{26}$Fe which fall with increasing energy up to ~100 GeV per amu and then level off at higher energies; from the energy dependence of these abundance ratios we infer Ar/Fe and Ca/Fe ratios in the source of $2.6 \pm 0.7\%$ and $8.8 \pm 0.7\%$, respectively.

Subject headings: cosmic rays: abundances

I. INTRODUCTION

The cosmic-ray particles arriving at Earth include a mixture of primary nuclei from the source and secondary nuclei which are fragmentation products of collisions with other nuclei such as those in the interstellar medium. Some elements, such as $_8$O, $_{14}$Si, $_{26}$Fe, and $_{28}$Ni, are predominantly primary; other elements, such as $_3$Li, $_4$Be, $_5$B, $_{19}$K, $_{21}$Sc, $_{22}$Ti, and $_{23}$V, are predominantly secondary; still other elements such as $_{18}$Ar and $_{20}$Ca, have significant components of both primary and secondary origin.

The secondary nuclei are produced as the primaries propagate from the source to Earth. A distribution of propagation path lengths is used in models of secondary production. In the simplest model which gives good agreement with observation, the distribution of path lengths is exponential (see, e.g., Brewster, Freier, and Waddington 1985). This path length distribution follows from a simple "leaky box model" in which cosmic rays have a small constant probability of leaking out of the Galaxy.

Up to ~10 GeV per amu, all primary elements are observed to have nearly the same energy spectra, while the secondary elements are observed to have steeper spectra. This difference between primary and secondary spectra was originally demonstrated by Juliusson, Meyer, and Muller (1972), Smith *et al.* (1973), Webber *et al.* (1973), and Balasubrahmanyan and Ormes (1973). The most precise measurements confirming these results, with energy spectra of individual elements over the wider interval from 1 to 25 GeV per amu, have come from the Danish-French experiment on *HEAO 3* (Engelmann *et al.* 1983). They find that the energy dependence of the ratio of abundances of various elements to the abundance of Si are well fitted by power laws in energy, E^p, with $-0.1 \leq p \leq 0.1$ for primary elements and $-0.3 \leq p \leq -0.2$ for secondary elements.

There are several reasons for extending these measurements of relative spectra to higher energies. First, the secondary-to-primary ratio is a measure of the mean path length in the leaky box model, and the fact that this ratio decreases with increasing energy implies that the higher energy cosmic-ray nuclei spend less time in the Galaxy than do those at lower energy. Thus, for example, it is possible that at higher energies the primary cosmic-ray nuclei come only from a subset of those sources which contribute at lower energies, and it is important to see whether the elemental composition from this subset of "high-energy" sources is the same as that from the full set. In any case, the observation of an energy-dependent composition would provide significant information about the source of cosmic-ray nuclei.

Second, if the mean path length continued to decrease with increasing rigidity, then at sufficiently high energy the cosmic-ray nuclei would traverse a considerably reduced amount of material and the observed composition would be very close to that of the source regions. Thus elements like $_{18}$Ar and $_{20}$Ca, which at lower energies are a mixture of primary and secondary components, would at higher energies be dominated by the primary component. At those lower energies, determination of the contribution due to the primary component requires subtraction of a substantial secondary component whose magnitude depends sensitively on the assumed propagation model and interaction cross sections. At higher energies the observed abundances would give the primary component, without this model-dependent subtraction.

Determination of the primary abundances of these elements is important to test models of fractionation of elemental abundances at the cosmic-ray source. In particular, it has been widely noted (see, e.g., Binns *et al.* 1984) that there is a significant source fractionation which is ordered by the first-ionization potential (FIP) of the elements. Among the lowest values of FIP is that of Ca, 6.1 eV, while Ar has a relatively

[1] Department of Physics and the McDonnell Center for the Space Sciences, Washington University, St. Louis.
[2] George W. Downs Laboratory, California Institute of Technology.
[3] School of Physics and Astronomy, University of Minnesota.

© American Astronomical Society • Provided by the NASA Astrophysics Data System

1988ApJ...324.1106B

high FIP, 15.8 eV; so the source abundances of these two elements are particularly important for constraining FIP models of source fractionation. Furthermore, measurements of these abundances above 100 GeV per amu will test whether the same FIP source fractionation applies at these very high energies as at lower energies. Thus these elements provide a further test of the possible energy dependence of primary element abundances.

Finally, if the secondary-to-primary abundance ratios were shown to deviate from simple power laws in energy, that would provide important information concerning the confinement and acceleration of cosmic-rays in the Galaxy. For example, it has been shown by Cowsik (1980) and Fransson and Epstein (1980) that a power-law decrease in the secondary-to-primary ratio over the interval from 1 to 100 GeV per amu severely limits the amount of cosmic-ray power which can be derived from a process in which the acceleration and the fragmentation occur in the same regions of space. This limitation was derived from observations of light elements, those with atomic number, Z, in the interval $3 \leq Z \leq 8$, and it should apply to heavier nuclei if they have a similar acceleration and propagation history.

Data from the Heavy-Nuclei Experiment (HNE) flown on *HEAO 3* allow us to extend the measurements of several cosmic-ray elements to much higher energies than previously measured. We have determined the abundances relative to $_{26}$Fe of the individual elements $_{18}$Ar, $_{19}$K, $_{20}$Ca, $_{21}$Sc, $_{22}$Ti, $_{23}$V, and $_{28}$Ni as a function of energy from 10 to several hundred GeV per amu. The best previous measurement in this charge and energy region (Simon *et al.* 1980) was severely limited by statistics, so spectra of individual elements were not measured. Having to combine all the elements in the interval $17 \leq Z \leq 25$, they were unable to see the differences in spectra of the various elements which we describe in this paper, although they did see the spectral difference between their predominantly secondary nuclei and the primary iron and nickel nuclei.

The HNE (Binns *et al.* 1981), which included ionization chambers, a Cherenkov detector, and multiwire ionization hodoscopes, was designed with the principal objective of measuring the elemental composition of the ultraheavy (UH) cosmic rays, those with Z greater than 30. However, this instrument was also suitable for the high-energy measurements at lower atomic numbers which we describe here.

The energy loss of charged particles in the gas of the ionization chambers exhibits a "relativistic rise," a logarithmic increase with increasing energy over the interval from a few GeV per amu to several hundred GeV per amu. We have used this relativistic rise to measure energies an order of magnitude greater than those measured by the Danish-French instrument on the same spacecraft. Because the fluxes of UH cosmic rays are very low, the HNE required a large exposure (area times solid angle times exposure time). This large exposure proved essential for the measurements reported here. While the elements with $Z < 30$ are relatively abundant compared with the UH elements, their steeply falling energy spectra demand very large exposure for measurements at the highest energies. The results reported here are derived from a subset of our data corresponding to an exposure of ~ 1 m^2 sr yr.

While the relativistic rise in multiwire proportional counters has been studied for singly charged particles using proton, pion, muon, and electron beams from particle accelerators (Cobb, Allison, and Bunch 1976; Allison and Cobb 1980), no such studies for heavy nuclei are available. Furthermore, in these studies of singly charged particles, the ionization measured by the counters was almost entirely due to passage of the particles through gas, while in the HNE ionization chambers part of the signal is due to knock-on electrons produced in the solid material above the ionization chambers, resulting in a distinctly lower relativistic rise.

Using balloon-borne ionization chambers similar to those in the HNE, Barthelmy (1985) and Barthelmy, Israel, and Klarmann (1985) have calibrated the relativistic rise for cosmic-ray Fe at 34 GeV per amu, the threshold of a gas Cherenkov dectector. In this paper, we derive an empirical calibration of the relativistic rise by comparing our observations of cosmic-ray Fe with energy spectra previously derived by other observers, and we show this calibration to be consistent with that derived by Barthelmy *et al.* We then apply this empirical calibration to other less abundant elements in the interval $18 \leq Z \leq 28$ for which no previous measurements for individual elements have been made.

This analysis is described in more detail by Jones (1985), and preliminary results from this analysis have also been described by Jones *et al.* (1985). The results in the present paper differ only slightly ($\sim 10\%$) from those preliminary results, due principally to correction of an error in the calculation of the effects of interactions in the detector system. In addition, for this paper we have evaluated the uncertainties caused by various assumptions in our analysis.

II. INSTRUMENTATION AND DATA SELECTION

a) Instrument Description

Figure 1 is a schematic cross section of the HNE. It is composed of six dual-gap ionization chambers, a Cherenkov detector, and four two-coordinate layers of multiwire ionization hodoscopes. The ionization chambers, three above and three below the Cherenkov detector, are filled with P-10 gas, 90% argon and 10% methane, at 1.1 atm absolute pressure. The Cherenkov detector is composed of two radiators of 0.5 cm thick Pilot-425, mounted on both sides of a light-diffusion box, viewed by eight photomultipliers. Each hodoscope layer has two crossed planes of collecting electrodes which consist of 124 or 156 parallel wires spaced 1 cm apart. The instrument has been described in more detail by Binns *et al.* (1981).

The instrument recorded the pulse height in each of the six ionization chambers and in each of the eight Cherenkov photomultipliers, and recorded the location of each hodoscope wire which collected an ionization signal greater than that expected from a minimum ionizing nucleus of Z greater than ~ 7–12. For the results presented in this paper we confined our analysis to the high-resolution subset of our data consisting of nuclei that penetrated both pieces of the Cherenkov detector radiator and all six ionization chambers while passing at least 7 cm from any chamber wall. The trigger threshold level in the ionization chambers was that of a minimum-ionizing nucleus of $Z = 17$ traveling perpendicular to the chamber electrodes, and the trigger threshold in the Cherenkov detector was that of a relativistic nucleus of $Z = 7$.

The *HEAO 3* spacecraft was spin oriented about an axis pointing toward the Sun, and the axis of our instrument was perpendicular to the spin axis. As a result, the orientation of the HNE with respect to Earth changed continuously during the flight in a known manner.

The spacecraft was launched on 1979 September 20, into a

© American Astronomical Society • Provided by the NASA Astrophysics Data System

1988ApJ...324.1106B

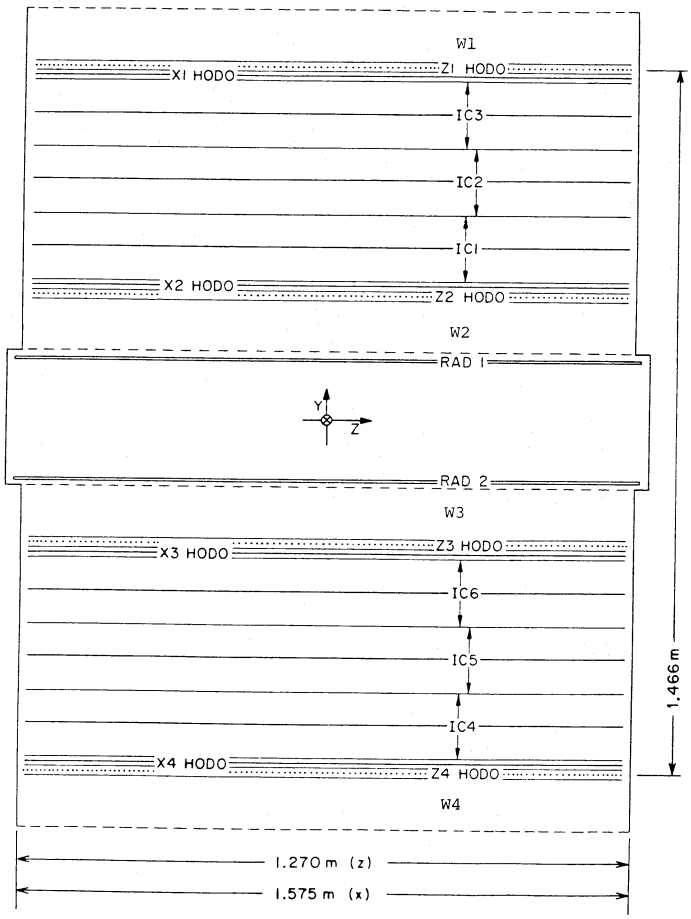

FIG. 1.—Schematic cross section of the *HEAO 3* heavy-nuclei experiment. "IC" are dual-gap ionization chambers, "RAD" are Pilot-425 Cherenkov radiators; "HODO" are layers of multiwire ionization hodoscopes; "W" are "windows" of aluminum honeycomb.

circular orbit at 500 km altitude and 43°.6 inclination, and it returned data until 1981 May 30. The analysis reported in this paper uses data of 314 days from 1979 September 25, shortly after the instrument was turned on, until the high voltage on two of the six ionization chambers failed.

b) Detector Response

The ionization hodoscope served to delineate the trajectory of each cosmic-ray nucleus though the instrument, and, when combined with the spacecraft orientation, defined the cosmic-ray trajectory relative to Earth. The symmetry of the HNE gave it a bidirectional response, and it did not distinguish between upward and downward moving particles. Only for calculated trajectories within 35° of the zenith (~13% of the events) were we confident that the sense of the particle motion was known; at larger angles we could not be certain that Earth shielded the instrument from one direction, because of the curvature of the particle trajectories in the geomagnetic field.

The particle trajectory relative to Earth and the location of the spacecraft were combined in a simple geomagnetic model to calculate the geomagnetic cutoff rigidity for each observed nucleus. For particles within 35° of the zenith an unambiguous direction was determined, and for the data presented in this paper we required that this cutoff be at least 8 GV. For the other particles, cutoffs were calculated for both possible directions, and we required that the lower of these two cutoffs be at least 8 GV.

The trajectory through the instrument was also used to correct the various pulse heights to the values they would have had if the particle had traveled along the instrument axis (perpendicular to the electrodes and through the center of the instrument). Each pulse height was multiplied by $\cos\theta$, where θ is the angle between the particle trajectory and the instrument axis, to correct for the angular dependence of the path length in each detector. Also each ionization chamber pulse height and the mean of the eight Cherenkov photomultiplier pulse heights was corrected by an empirical factor depending on the location where the particle crossed the center plane of each detector; this area correction was determined from an analysis of the inflight data from the abundant cosmic-ray Fe nuclei (Binns *et al.* 1981). In all the following discussions the ionization and Cherenkov signals are those which result from applying these corrections to the raw data.

A useful approximation for the most probable value of the Cherenkov signal, C, is

$$C = Z^2\left(1 - \frac{1}{\beta^2 n^2}\right)\Big/\left(1 - \frac{1}{n^2}\right),$$

where β is the particle velocity in units of the velocity of light and n is the effective index of refraction of the Cherenkov radiator. The factor in the denominator serves to normalize C to the value Z^2 when $\beta = 1$. In the data analysis it is convenient to work with the square root of the Cherenkov signal, and we define

$$Z_C = \sqrt{C}\,.$$

(In our analysis, Cherenkov signals are normalized so that Z_C thus defined is in charge units [cu], with Z_C being very nearly equal to Z for β near unity.) The cosmic-ray nuclei used here have $\beta > 0.97$ since they were selected to have cutoff rigidity at least 8 GV (corresponding to 2.9 GeV per amu for ^{56}Fe or 3.2 GeV per amu for ^{40}Ca). Consequently Z_C is a good measure of the atomic number, Z.

The most probable ionization chamber signal I can be described by the expression

$$I = Z^2\,\frac{f(\beta)}{f(0.96)}\,.$$

The function $f(\beta)$ has a broad minimum near $\beta = 0.96$ (2.5 GeV per amu) and rises at higher energies approximately as the logarithm of the energy until it saturates and becomes independent of energy above several hundred GeV per amu. The factor in the denominator serves to normalize I to the value Z^2 at the minimum. In the data analysis it is convenient to work with the square root of ionization signal, and we define

$$Z_I = \sqrt{I}\,.$$

(In our analysis, ionization signals are normalized so that Z_I thus defined is in charge units, with Z_I being very nearly equal to Z for a minimum ionizing nucleus.) Since the cosmic-ray nuclei selected for this paper all have $\beta > 0.97$, they are in the region where Z_I increases approximately logarithmically with increasing energy.

Thus in this paper the atomic number of each nucleus is determined from Z_C and the energy is derived from the rela-

© American Astronomical Society • Provided by the NASA Astrophysics Data System

1988ApJ...324.1106B

tivistic rise, ρ, defined by

$$\rho = \frac{Z_I}{Z} .$$

We assume that over the range of atomic numbers considered here, $18 \leq Z \leq 28$, ρ is a function only of the velocity (or energy per nucleon).

c) *Data Selection*

In addition to selecting only particles observed at cutoff rigidities greater than 8 GV, data were also subjected to several internal consistency checks before being included in this analysis. These checks served to exclude most of the nuclei which suffered nuclear interactions inside the instrument and to exclude events in which an extraneous particle, in coincidence with another, added to the signal in one or more of the ionization chambers or in one or more of the photomultipliers.

The most significant selection was designed to eliminate nuclear interactions in the material between the two sets of three ionization chambers. This material includes the 1.14 g cm^{-2} of plastic Cherenkov radiator and 1.40 g cm^{-2} of aluminum honeycomb on each side of the Cherenkov detector, which was part of the pressure vessel containing the ionization chamber gas. We required the absolute value of ΔZ_I, the difference between Z_I determined from the mean of the signals in chambers IC1, IC2, IC3 (Z_{IA}) and that from chambers IC4, IC5, IC6 (Z_{IB}), to be less than 6% of Z_C:

$$\frac{|\Delta Z_I|}{Z_C} = \frac{|Z_{IA} - Z_{IB}|}{Z_C} < 0.06 .$$

This criterion is roughly the same as requiring that ΔZ_I is less than 1.5 cu.

For particles whose direction of incidence is known, those which first traversed chambers IC1, IC2, IC3 were found to have a peak in ΔZ_I centered at about -0.5 cu with a standard deviation of ~ 0.8 cu while those which first traversed chambers IC4, IC5, IC6 had a peak centered at about $+0.5$ cu. This difference was presumably due to extra knock-on electrons in the material between the two sets of ionization chambers. For particles with zenith angle greater than 35° the direction was uncertain, with about the same total numer entering each side, so the distribution was wider and centered at zero.

The effect of requiring $|\Delta Z_I|/Z_C < 0.06$ was to eliminate nearly all those nuclei which interacted between the two sets of ionization chambers and changed charge by at least 3 cu, approximately half of those which changed charge by 2 cu, and a few percent of those which changed charge by only 1 cu or did not interact. In addition, this criterion would be expected to eliminate most events in which a second particle from another direction penetrates a portion of the detector system within the electronic resolving time of the instrument. This criterion rejected 23% of all events, consistent with known interaction probabilities in the amount of material which was present.

Of the remaining events, 4% were rejected by requiring agreement among the three ionization chambers in each half of the instrument. We required that the rms of the difference between the Z_I of the first two ionization chambers and that of the second two be less than 0.1 of the Z_I calculated from the mean of the three. This criterion was instituted to eliminate most of the remaining coincidences with extraneous particles.

Then 2% of the remaining events were rejected by a complex criterion on the agreement among the eight photomultiplier pulse heights. This criterion was designed to eliminate events in which one photomultiplier registered an anomalously high pulse height because it had been hit by an extraneous particle.

As a check on the consistency of the various pulse heights, we required $Z_C/Z_I < 1.05$. By definition the most probable value of Z_C/Z_I is always less than unity. Taking account of the instrumental resolution in Z_C and Z_I, this ratio should rarely exceed 1.05. In fact, only 0.01% of the remaining events failed this criterion.

III. ANALYSIS

a) *Raw Abundances*

Figure 2 is a plot of Z_C versus Z_I showing the locus of events for each element in the interval $20 \leq Z \leq 28$; each locus is nearly a vertical line. We analyze the data by working with histograms of Z_C for particles in narrow intervals of Z_I. The dashed lines in Figure 2 locate six such intervals, and Figure 3 shows the Z_C histograms for the particles in each of these representative intervals. For example, Figure 3*a*, the Z_C histogram for $29.3 < Z_I < 29.5$ includes $_{26}$Fe, $_{27}$Co, and $_{28}$Ni at mean energies of ~ 130, ~ 34, and ~ 12 GeV per amu respectively. Eighty such histograms were analyzed, each covering an interval of 0.2 cu in Z_I, for values of Z_I ranging from 17.5 to 33.5 cu. In each histogram which displayed a peak due to $_{26}$Fe, the mean value of Z_C for $_{26}$Fe was determined by fitting a Gaussian to the data. The Fe line in Figure 2 is a plot of the resulting mean value of Z_C as a function of Z_I. The other lines in Figure 2 are derived by simple Z scaling from the Fe line.

The abundance of each element in each of the histograms was determined by maximum-likelihood fitting (Awaya 1979;

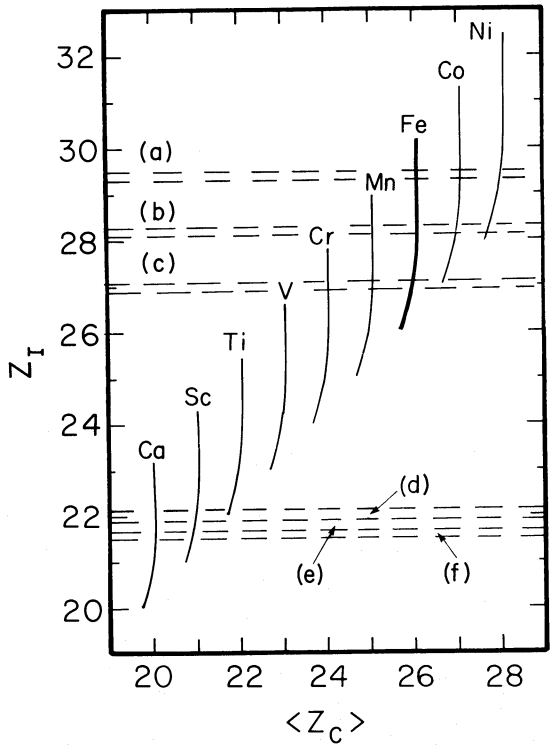

FIG. 2.—Mean value of Z_C as a function of Z_I for each element in the interval $20 \leq Z \leq 28$. Dashed lines indicate the intervals of Z_I displayed in Fig. 3.

© American Astronomical Society • Provided by the NASA Astrophysics Data System

1988ApJ...324.1106B

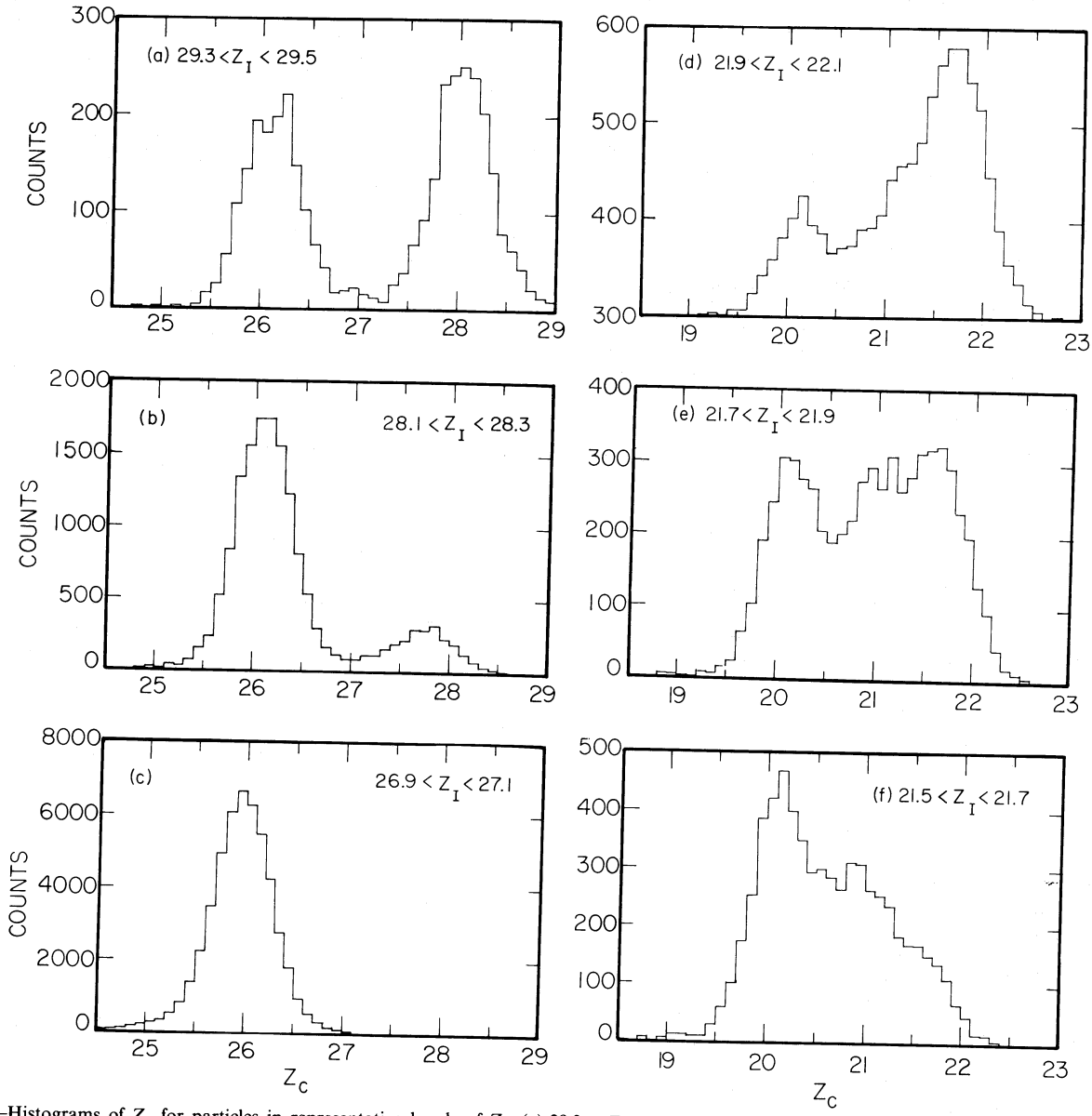

FIG. 3.—Histograms of Z_C for particles in representative bands of Z_I. (*a*) $29.3 < Z_I < 29.5$. (*b*) $28.1 < Z_I < 28.3$. (*c*) $26.9 \leq Z_I < 27.1$. (*d*) $21.9 < Z_I < 22.1$. (*e*) $21.7 < Z_I < 21.9$. (*f*) $21.5 < Z_I < 21.7$.

Bakers and Cousins 1984). The events assigned to each element were assumed to be distributed in a Gaussian distribution about the mean of Z_C shown in Figure 2. The fitting results confirmed that each element peak was indeed at the predicted location within 0.03 cu. Initially the standard deviation, σ, of the Gaussian fits was taken as a free parameter. The resulting values of σ were all in close agreement, and the final abundances in each peak were derived from fits with σ fixed at the mean value of 0.285 cu. The result of this fitting was a set of "raw" abundances of individual elements, $18 \leq Z \leq 28$, in these narrow Z_I bins; abundances for each element were typically determined over the interval of Z_I from $\sim 0.97Z$ to $1.15Z$. (In further analysis we did not use peaks whose fit abundances were less than 10% of an adjacent peak, because such abundances could depend sensitively on the shape of the fitting function. We also did not use "peaks" defined by fewer than 10 events).

b) Energy Scale

We used the relativistic rise, $\rho = Z_I/Z$, as a measure of energy, where Z_I was determined from the mean of the six ionization chambers. We derived an empirical calibration of ρ by comparing our Fe observations with a differential Fe energy spectrum derived from a compilation of previously published measurements.

The starting point is the number of Fe events found by fitting the peaks in each of the Z_C histograms in the interval $24.9 < Z_I < 31.3$. The data points in Figure 4 give the number of Fe events in each histogram. The points are plotted at the value of ρ corresponding to the midpoint of each Z_I bin. The error bars indicate the statistical uncertainty in the observed numbers.

The empirical Fe spectrum which we adopted (Webber 1983) is shown as the solid line in Figure 5. Above 300 GeV per amu,

© American Astronomical Society • Provided by the NASA Astrophysics Data System

1988ApJ...324.1106B

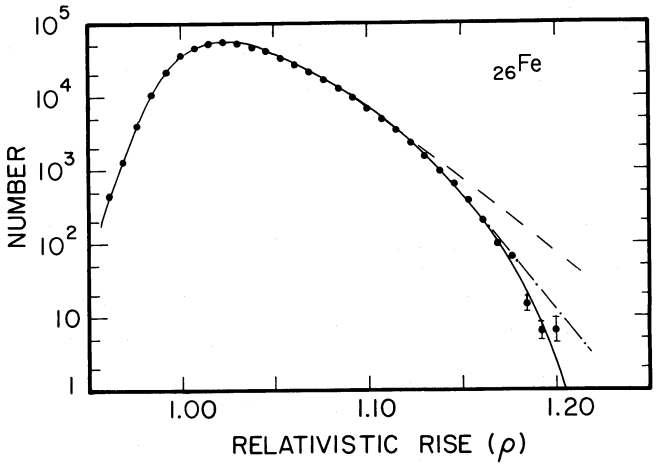

FIG. 4.—*Data points*: number of Fe nuclei as a function of relativistic rise, ρ (Z_I/Z). *Curves*: calculated Fe (normalized to the observed number of Fe near the peak) using corresponding ρ calibration curves from Fig. 6.

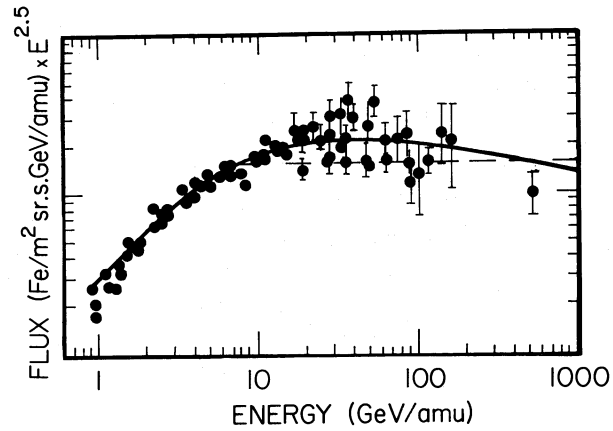

FIG. 5.—Cosmic-ray Fe energy spectrum. Data points are from various measurements, as compiled by Webber (1985). Solid curve is adopted Fe energy spectrum. Dashed curve is alternative Fe energy spectrum.

where there are essentially no data, we assumed that the spectrum continued as energy to the power -2.7. (An alternative Fe spectrum that goes as energy to the power -2.5 at all energies above 8 GeV per amu is shown as a dashed line in Figure 5. As discussed below in § IV, our final conclusions were very insensitive to which of these Fe spectra was adopted.) This Fe spectrum was multiplied by an empirical geomagnetic transmission function (Jones 1985) which represented the fraction of time when the geomagnetic cutoff permitted Fe nuclei of that energy to reach the instrument, including the fact that data were used only if the geomagnetic cutoff was above 8 GV; the product was the effective Fe energy spectrum at the instrument, averaged over many orbits. This energy spectrum was then converted to a ρ spectrum using a trial form of the energy dependence of ρ. We found that a form composed of simple logarithmic segments was an adequate approximation. Finally, this calculated spectrum was folded with the instrument's ionization resolution (standard deviation in Z_I of 0.40 cu), and the resulting ρ spectrum was compared with the data. The process was iterated, by changing the assumed form of the energy dependence of ρ until the calculated and observed ρ spectra of Fe agreed.

The solid line in Figure 6 shows the empirical calibration of ρ which was thus derived; this is the calibration adopted for the remainder of the data analysis. The solid curve through the data points in Figure 4 is derived from this calibration and gives an excellent fit to the observed Fe data. The dashed and the dash-dotted lines in Figure 4 show the results for the corresponding alternative calibration curves in Figure 6. The dashed calibration curve, with no break at 50 GeV per amu, is clearly wrong. Various forms for the rolloff in ρ at the highest energies, such as a change of slope at 440 GeV per amu, could also fit the data, but the conclusions in this paper are insensitive to the assumed shape of this rolloff. Indeed, for ρ above ~ 1.15 the shape of the curve in Figure 4 is dominated by the resolution function and is quite insensitive to changes in the shape of either the calibration curve, or the assumed shape of the Fe energy spectrum above 300 GeV per amu. We also note that the results in this paper, which are only for energies above 10 GeV per amu, are insensitive to the detailed shape of the assumed geomagnetic transmission function, because it is only below this energy that the transmission function differs appreciably from unity.

In Figure 6, the open circle is a calibration point derived by Barthelmy, Israel, and Klarmann (1985) for ionization chambers similar to those used in the HNE. This calibration was based on a comparison between signals from cosmic-ray Fe in the ionization chambers and in a gas-Cherenkov detector (carbon dioxide at 1 atm) whose threshold was 34 GeV per amu. This point is very well defined by the data; the uncertainties are smaller than the plotted symbol. We believe that this point lies below our curve because the ionization chambers used by Barthelmy *et al.* had significantly less material in the detector array, resulting in fewer knock-on electrons in the ionization chambers. This supposition is confirmed by looking at the calibration derived for Z_I of only the first three ionization chambers (using only events for which the particle direction was known), as indicated by the series of crosses on Figure 6. The material in front of these three HNE ionization chambers was 1.2 g cm^{-2}. In the Barthelmy *et al.* instrument the

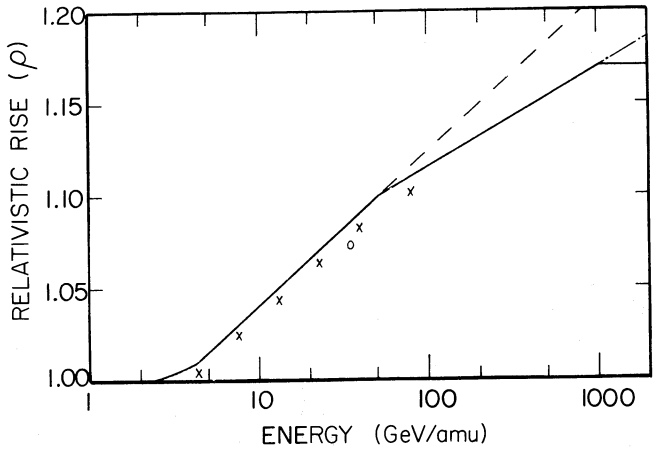

FIG. 6.—Calibration of relativistic rise (ρ) as a function of energy. Solid line is the adopted calibration. Dashed and dot-dashed lines are alternate calibrations which were tested. Open circle (○) is calibration from Barthelmy (1985). Crosses (X) indicate the calibration for the front chambers of the HNE.

© American Astronomical Society • Provided by the NASA Astrophysics Data System

1988ApJ...324.1106B

ionization measurement was the mean of three chambers, which had, respectively 0.40, 1.5, and 2.4 g cm^{-2} of matter in front of them; so the mean amount of material in front of these chambers was 1.4 g cm^{-2}, nearly the same as for the first three HNE chambers. We note that the calibration point measured by Barthelmy *et al.* and the empirical calibration curve derived here differ by $\sim$15%, an indication of the uncertainty in the energy calibration for Fe at energies below $\sim$100 GeV per amu. The energy resolution, however, is much poorer, as described below.

The calibration indicated by the solid curve in Figure 6 applies only to our instrument and cannot be taken as generally applicable to relativistic rise in gas detectors. The signal observed in our ionization chambers is partly the result of energy loss in the gas of these chambers and partly the result of high-energy knock-on electrons created in the solid material above the chambers, for which the relativistic rise would be expected to have a different energy dependence.

In applying the calibration curve during data analysis, two effects of the finite ionization resolution must be taken into account. First, the events observed with a particular value of the relativistic rise, ρ, come from a wide range of energies. The slope of the solid curve in Figure 6 implies that the Z_I resolution, standard deviation 0.40 cu, corresponds to a factor of 1.5 in energy below 50 GeV per amu and a factor of 1.9 above this energy.

Second, when the finite resolution and the steep energy spectrum are taken into account we find that the mean energy of particles observed in any ρ bin is significantly lower than that corresponding to the center of the bin; in fact, for the narrow bins used in this analysis (0.2 cu in Z_I) the mean energy of particles observed in a bin lies below the energy corresponding to the lower edge of that bin. The light solid line in Figure 7 shows, as a function of the relativistic rise, ρ, the mean energy for particles observed within a bin of width 0.2 cu in Z_I centered at that value of ρ, using our assumed energy spectrum for Fe. Since secondary elements are observed to have a steeper energy spectrum, the mean energy corresponding to the same value of ρ is slightly different for each element. For example, the dashed curve in Figure 7 shows the mean energy for an element whose spectrum is steeper than that of Fe by a factor $E^{-0.28}$, the relative spectrum we find for Ti. In the following

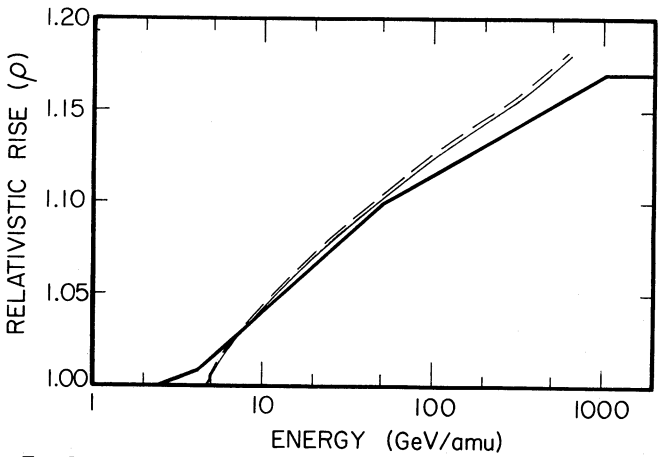

FIG. 7.—Mean energy of Fe (*light solid line*) or Ti (*dashed line*) events observed in a narrow bin centered at ρ. For reference, the heavy solid line is the same as the solid line in Fig. 6.

data analysis, the energy corresponding to data at a given value of ρ is taken from this light solid line for Fe, and from the appropriate corresponding curve for the other elements.

c) *Energy Dependence of Relative Abundances*

As described in § III*a* above, we determined the number of events due to each element in each of the 0.2 cu wide intervals of Z_I. The result is a set of raw abundances for various (Z, ρ). Before using these numbers, corrections for interactions in the detector system were necessary.

For each (Z, ρ) bin, starting at the highest Z, we calculated how many events must have been lost from the bin because of nuclear interactions in each of many thin layers of detector material, and we corrected the observed number by adding this number of interacted nuclei. For each of these interacted nuclei we calculated the probability that the interaction product gives signals in the instrument that would be identified as a particle meeting our selection criteria in one of the other (lower Z) bins. We then subtracted the appropriate number from the observed number in each of those bins. In the case of interactions in the honeycomb lid in front of the first ionization chamber, all lower Z bins were affected; for interactions inside the detector system the ΔZ_I agreement criterion limited the effect on lower bins to those which could be reached by interactions with charge change less than 3 cu.

In these calculations we used the total charge changing cross sections of Westfall *et al.* (1979). For the partial cross sections we used measurements by Webber (1985) for Fe at 1.6 GeV per amu interacting in carbon and in polyethylene, and his inferred cross sections for hydrogen. We have assumed that the ratio of the partial cross section for a given ΔZ to the total cross section is the same for all other interacting elements as it is for Fe. The Webber cross sections apply to charge changes before decay of unstable secondaries (Webber and Brautigam 1982), which is appropriate for interactions in the detector system. For interactions in the aluminum components of our detector system we used the measured ratios of partial to total cross sections for carbon, and for interactions in the Cherenkov radiator we combined the carbon and hydrogen cross sections under the approximation that the composition of Plexiglas is CH. We used cross sections for 1.6 GeV per amu because that is the highest energy at which such cross sections have been measured, and there is evidence (Webber 1985) that these cross sections are relatively insensitive to energy above 1 GeV per amu. However, we recognize that the interactions of interest to us occur at energies about two orders of magnitude higher, and we indicate below the sensitivity of our results to those assumed partial cross sections.

Although the individual interaction probabilities are not very high, in some cases the interaction correction is substantial because the abundance of correctly identified particles in a particular (Z, ρ) bin may be much less than the abundance in the bin from which misidentified particles originate. For example, if a 50 GeV per amu $_{26}$Fe nucleus interacts, changing charge by 2 cu in the material between the upper ionization chambers and the Cherenkov detector, it would result in $Z_C = 24$, and so would be assigned $Z = 24$, but the assigned value of Z_I would be the mean of the Z_I corresponding to a 50 GeV per amu $_{26}$Fe and that corresponding to a 50 GeV per amu $_{24}$Cr. This particle would thus be assigned ρ (Z_I/Z) corresponding to an energy of $\sim$300 GeV per amu. Thus an interacting 50 GeV per amu $_{26}$Fe would be misidentified as a 300 GeV per amu $_{24}$Cr. The ΔZ agreement criterion would elimi-

© American Astronomical Society • Provided by the NASA Astrophysics Data System

1988ApJ...324.1106B

nate only half these interactions. Not only is $_{26}$Fe more abundant than $_{24}$Cr at the same energy, but also the abundance at 50 GeV per amu is much greater than at 300 GeV per amu, so the result is a very large interaction correction for $_{24}$Cr. Although the corrections for Cr are large, the corrected ratio is nevertheless quite plausible, lending credence to our interaction calculation. For $_{25}$Mn and $_{27}$Co the corrections are so large as to make it impossible to draw any meaningful conclusions for these two elements. The magnitude of the interaction corrections for the other elements are indicated below.

The corrected abundances for each (Z, ρ) bin were then divided by the number in the Fe bin at the ρ corresponding to the same energy. Since the Fe bins were generally not at exactly the same energies as the bins for any other element, the Fe abundance corresponding to that of some other element was found by simple two-point interpolation between bins. Since the width in Z_I of all bins for all elements was 0.2 cu, each ratio was multiplied by $Z/26$ to compensate for the different widths in ρ of the bins for the two elements.

In figures 8, 9, and 10 we plot the resulting abundances relative to Fe. Also shown are the results from the Danish-French experiment on the same spacecraft (Engelmann *et al.* 1983). The two sets of data display good agreement in the energy interval where they overlap, 10–25 GeV per amu.

The error bars on our data in these figures are statistical only and do not include uncertainty due to the interaction corrections. To indicate the sensitivity of our results to this uncertainty, we also show with light lines the locations of our data points under two extreme assumptions.

For the upper line, the raw data have been corrected only for the loss of nuclei due to interactions, but no correction has been made for the gain of nuclei in a bin due to interactions of higher Z nuclei. This correction is equivalent to assuming that whenever these nuclei interact, the charges of the fragments are so small as to remove the event from our analysis. Since the loss of nuclei due to interactions is nearly the same for all the elements we consider, the abundance *ratios* which are plotted here are very weakly affected by this correction, and so the upper line is very nearly the one which would be derived from the raw data, without any correction for interactions in the detector. This line surely represents an upper limit to the measured abundances.

The lower line is a plot of the corrected abundances, assuming arbitrarily that all the partial cross sections affecting these data are increased by a factor of 1.5. We believe that this line is a conservative lower limit to the plotted abundances.

For clarity no horizontal error bars are plotted in these figures, but, as described in the previous section, these data points are separated by 0.2 cu in ionization, while the ionization resolution is 0.4 cu. Thus while each point is plotted at the mean energy of the particles contributing to this point, these particles are in fact spread over energies extending approximately two points on either side. As a result our measurements would be less sensitive to sharp spectral features than the spacing of the data points would suggest; but, on the assumption of smooth spectra, the spectral slopes derived from these data should be correct.

IV. DISCUSSION

a) Nickel

Since Ni and Fe are both primary elements, we expect their abundance ratio to be nearly independent of energy if the composition of the high-energy sources is the same as that of the lower energy sources. Our data (Fig. 8) suggest that between 10 and 500 GeV per amu the Ni/Fe ratio is slightly dependent upon energy, with a best-fit power law of exponent -0.050 ± 0.016. If we ignore this slight variation with energy, then our data give a mean value of the Ni/Fe ratio above 10 GeV per amu of 0.054 ± 0.001. The result is in agreement with the highest energy points of the Danish-French experiment. However, the data of that experiment do suggest an energy dependence of this ratio, rising from $\sim$0.045 at $\sim$1 GeV per amu to $\sim$0.055 at $\sim$10 GeV per amu. Data from our HNE at low energies, between 0.5 and 1 GeV per amu, (Israel *et al.* 1983; Jones 1985) also indicates a Ni/Fe ratio of $\sim$0.045 below 1 GeV per amu.

b) Pure Secondary Nuclei

For the secondary ratios, K/Fe, Sc/Fe, Ti/Fe, and V/Fe (Fig. 9), our data indicate an extension to $\sim$150 GeV per amu of the

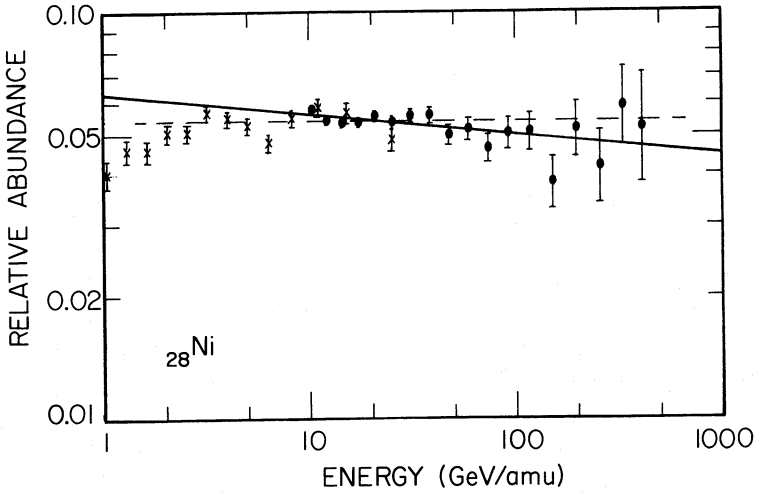

FIG. 8.—Abundance of Ni relative to Fe (Ni/Fe ratio) vs. energy. Filled circles (●) are data from this experiment; crosses (X) are data from Engelmann *et al.* (1983). Statistical uncertainties are indicated only where they are larger than the plotted points. Solid line is power-law fit to data from this experiment only. Dashed line is mean value for all data from this experiment.

© American Astronomical Society • Provided by the NASA Astrophysics Data System

1988ApJ...324.1106B

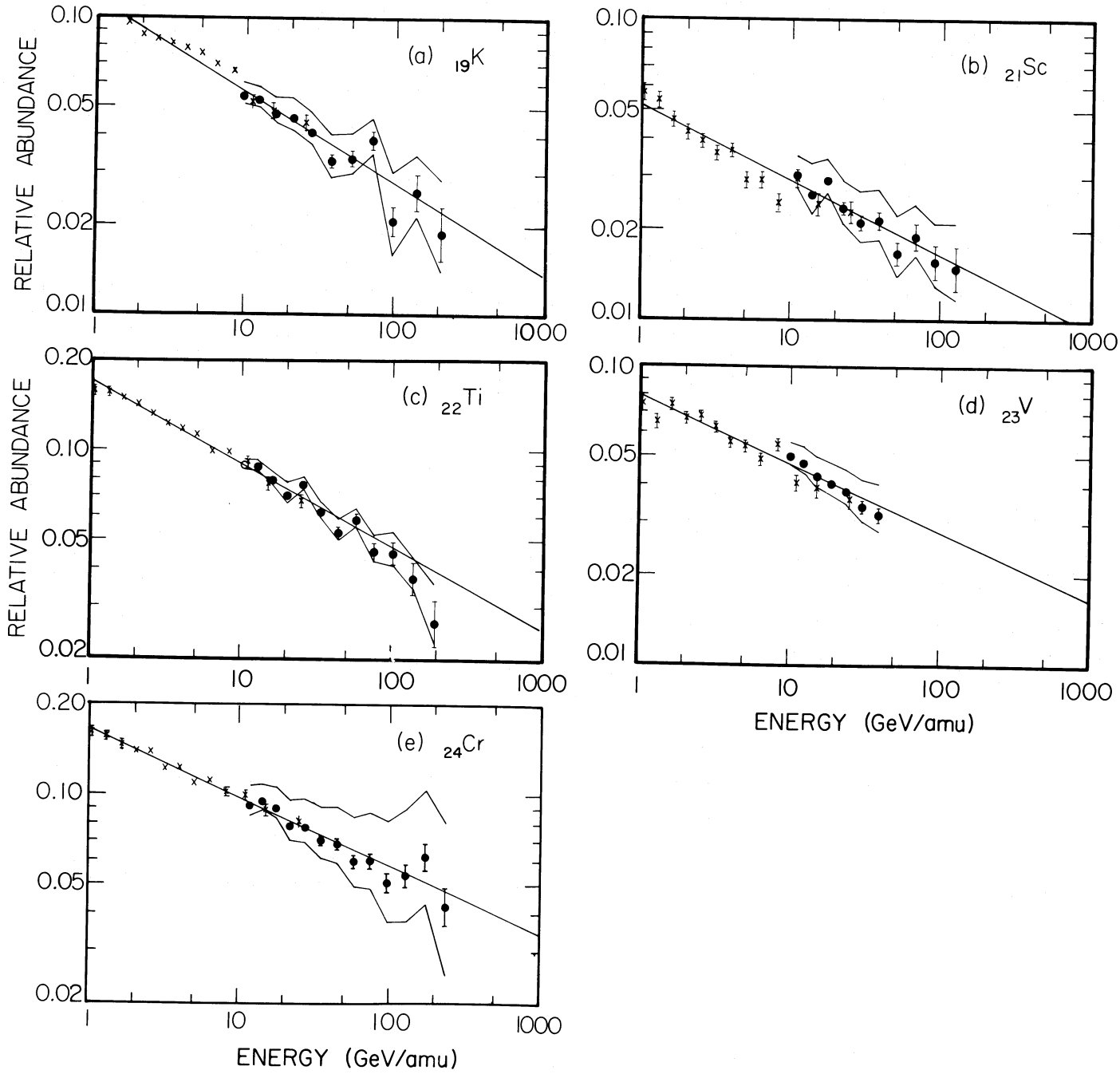

FIG. 9.—Abundances of secondary elements relative to Fe. (*a*) K/Fe ratio; (*b*) Sc/Fe ratio; (*c*) Ti/Fe ratio; (*d*) V/Fe ratio; (*e*) Cr/Fe ratio. Filled circles (●) are data from this experiment; crosses (X) are data from Engelmann *et al.* (1983). Light broken lines are limits on our data under extreme assumptions concerning interaction corrections, as discussed in the text. Solid line is power-law fit to all plotted data, from both experiments.

same power-law dependence as that indicated by the Danish-French data. The best fit exponents for these four ratios, combining all the data plotted here from both experiments, are, respectively, -0.31 ± 0.01, -0.25 ± 0.02, -0.28 ± 0.01, and -0.23 ± 0.02. The fits which give these exponents have values of reduced chi-squared (χ_r^2) between 2.0 and 2.5, suggesting that the errors on the data points are underestimated; consequently, the uncertainties given here are the formal fitting errors multiplied by a factor $(\chi_r^2)^{1/2}$. These exponents, and a linear least-squares fit to them, are plotted in Figure 11. The variation of the exponent with Z is expected since elements with lower Z have greater contributions from interactions of secondary nuclei.

Data for the secondary ratio Cr/Fe are included in Figure 9, and the resulting exponent is included in Figure 11, to lend support for the calculation of the interaction correction. Because the interaction corrections for $_{24}$Cr are significantly larger than for the other elements, the Cr point was not included in deriving the Z dependence of the exponents; however, it is apparent from the figure that inclusion of this point would not change this Z dependence.

These results are insensitive to the details of the relativistic

© American Astronomical Society • Provided by the NASA Astrophysics Data System

1988ApJ...324.1106B

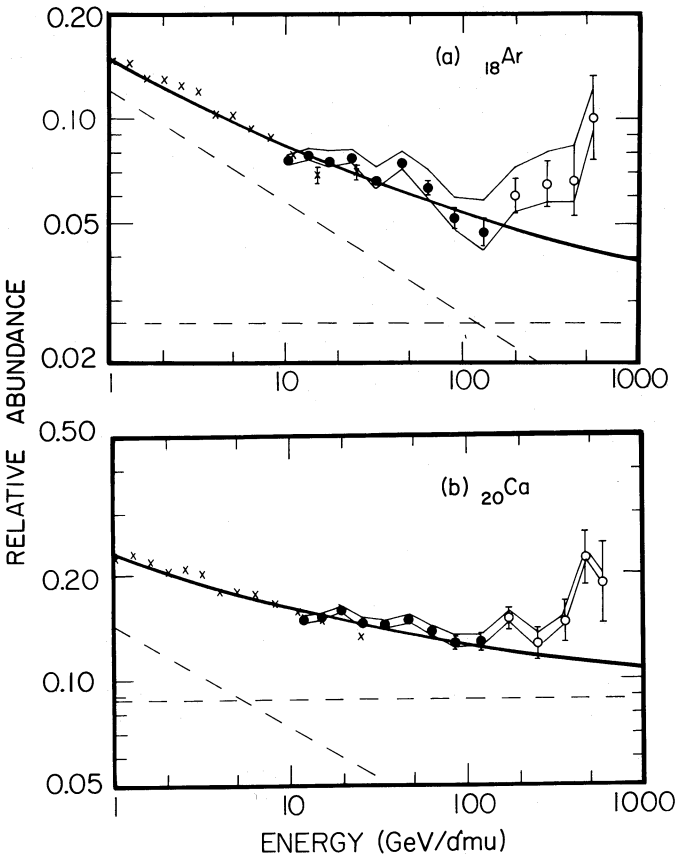

FIG. 10.—Abundances relative to Fe of elements with primary and secondary components. (*a*) Ar/Fe ratio; (*b*) Ca/Fe ratio. Filled circles (●) and open circles (○) are data from this experiment, crosses (X) are data from Engelmann *et al.* (1983). Light broken lines are limits on our data under extreme assumptions concerning interaction corrections, as discussed in the text. Solid line is fitted to data from both experiments, omitting open circles, using a power law plus a constant, with exponent of the power law inferred from Fig. 11. Dashed lines display separately the power law and the constant terms of this fit.

rise analysis described above in § III*b*. For example, adopting the alternative Fe energy spectrum in Figure 5 changes the calibration curve of Figures 6 and 7 slightly, but the resulting best-fit exponent for Ti/Fe changes only from 0.277 to 0.284.

The present results on the ratios of the secondary elements K, Sc, Ti, and V to their progenitor Fe reinforce previous constraints on models of cosmic-ray acceleration. The previously observed power-law decrease in the secondary-to-primary ratio (Li + Be + B)/(C + O) or (Li + Be + B + N)/(C + O) were shown by Cowsik (1980) to be inconsistent, to second order, with the continuous acceleration of cosmic rays in a Fermi-like process. Such a model of acceleration results in an increase of the secondary-to-primary ratio with energy. Eichler (1980) and Fransson and Epstein (1980) independently discussed models of interstellar acceleration. Neither model allows a decrease of more than a factor of 2 in the secondary-to-primary ratio before leveling off at high energies. Cowsik (1986) has discussed reacceleration of cosmic rays by shock waves and has shown that the observed decrease with energy of the secondary-to-primary ratio is inconsistent with substantial gains in energy, except at very low energies. Wandel *et al.* (1987) discuss reacceleration for particles arriving with energies below those considered in this paper. Our present results show distinctly more than a factor of 2 change in the ratio, as well as showing no evidence of leveling off up to ~150 GeV per amu. They reinforce the conclusions of Cowsik (1986) by extending the observation to heavier elements.

Peters and Westergaard (1977) have suggested a closed Galaxy model which affects the secondary-to-primary ratios at very high energies. However, for these heavy nuclei the predictions of this closed Galaxy model are indistinguishable from those of the standard leaky box model below ~300 GeV per amu, and we were limited by counting statistics from extending our measurements on secondary nuclei above 200 GeV per amu.

c) Calcium and Argon

Our data for the Ar/Fe and Ca/Fe ratios (Fig. 10) indicate a leveling above the energies of the Danish-French experiment, as would be expected for an energy-independent primary component that becomes increasingly significant at higher energies as the secondary component becomes less abundant. We fitted the combined data from the two experiments to a function $aE^p + b$, where b is the primary component and p was interpolated from Figure 11. With $p = -0.321 \pm 0.028$ for Ar/Fe and $p = -0.291 \pm 0.010$ for Ca/Fe, we get primary abundance ratios of Ar/Fe = 0.026 ± 0.007 and Ca/Fe = 0.088 ± 0.007. The uncertainties given here are again the formal fitting errors multiplied by a factor $(\chi_r^2)^{1/2}$. The uncertainty on the abundance ratios is the quadratic sum of the uncertainty derived from a fit with the assumed value of p and the variation in the fit as this assumed value varies over its uncertainty.

Like the secondary exponents discussed above, these results were very insensitive to the relativistic rise analysis described above in § III*b*, changing by less than 0.001 when the alternative Fe energy spectrum was used. The primary abundance ratios were also insensitive to whether or not we included our five highest energy points in the fitting, due to their low statistical weight. The primary ratios differed by 0.002 between fits with and without these points, and the values quoted are for the fits which omit these points. Our primary ratios do depend, but not very sensitively, upon the assumed value of the secondary exponent, p. Changing p from the interpolated values from Figure 11 to -0.31, the value for $_{19}$K, changes the inferred Ar/Fe primary ratio from 0.026 to 0.024 and the Ca/Fe primary ratio from 0.088 to 0.092.

A galactic propagation calculation on the Danish-French data (Lund 1984) gives a source abundance of Ar/

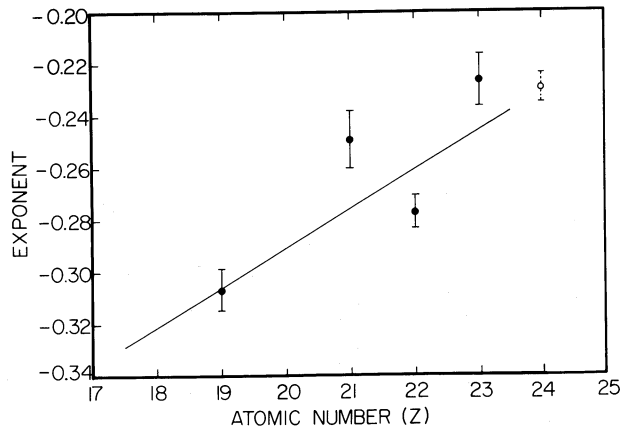

FIG. 11.—Best-fit exponent for the power laws in Fig 9. Solid line is the linear least-squares fit to the four points plotted as filled circles (●).

© American Astronomical Society • Provided by the NASA Astrophysics Data System

1988ApJ...324.1106B

Fe = 0.032 ± 0.008 and of Ca/Fe = 0.065 ± 0.019. The results of Krombel and Wiedenbeck (1985) on the isotope ^{40}Ca, which is mainly primary, give a source abundance of this isotope of ^{40}Ca/Fe = 0.070 ± 0.017; this is taken as a good measure of the elemental Ca/Fe ratio since the source Ca is expected to be almost pure ^{40}Ca. Our result and these other results, each divided by the "solar system" value of 0.0679 (Anders and Ebihara 1982) are displayed in Figure 12. This figure demonstrates that the three different approaches to determining the Ca/Fe source ratio are in reasonable agreement, as are the two different approaches to the Ar/Fe source ratio.

The first ionization potential of Ca is 6.1 eV, distinctly lower than that of Fe (7.9 eV), while that of Ar is 15.8 eV, substantially higher than Fe. Thus the primary abundance ratios we have derived for these elements confirm the inverse correlation between source abundances and first ionization potential which has previously been noted by many authors (see e.g., Binns *et al.* 1984). Since our results for the primary components come from fitting observations over a wide range of energies, it is difficult to assign a specific energy to our derived ratios. However, we note that in the neighborhood of 100 GeV per amu our observed Ar/Fe ratio is less than 0.06, so without any further analysis we can state that at 100 GeV per amu the primary Ar/Fe ratio is less than this value. Since this value is half the solar system value (see upper limit plotted in Fig. 12), we have direct evidence that 100 GeV per amu nuclei have been affected by first-ionization fractionation.

For comparison, we also display in Figure 12 the coronal Ca/Fe and Ar/Fe abundance ratios (Breneman and Stone 1985), again divided by the "solar system" values of these ratios. These coronal abundances were derived from their measurements of solar energetic particle element abundances from 10 solar flares. They corrected for a flare-to-flare variability, which exhibits a monotonic dependence on the ionic charge-to-mass ratio, to derive coronal abundances; these are the "source abundances" for the solar energetic particles, and displays a remarkable similarity to the source abundances for Galactic cosmic rays.

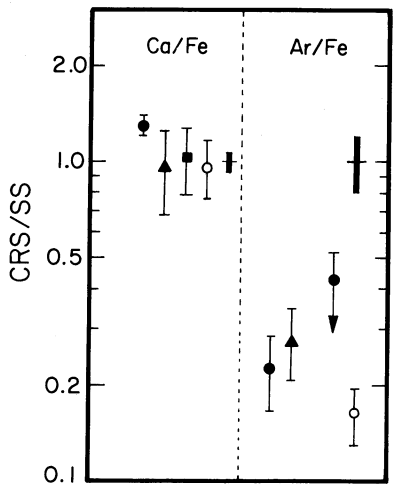

FIG. 12.—Cosmic-ray source ratio divided by "solar system" ratio (Anders and Ebihara 1982) for Ca/Fe and for Ar/Fe. Filled points are for galactic cosmic rays: Filled circles (●) represent data from this experiment; Filled triangles (▲) data from Lund (1984); Filled square (■) data from Krombel and Wiedenbeck (1985). Open circles (○) are for solar energetic particles (Breneman and Stone 1985). Error bars plotted on data points ignore uncertainties in the solar-system ratio. Solid bars centered at 1.0 indicate uncertainties of solar-system ratios. The upper limit (↓) for the Ar/Fe ratio is based on the lowest observed point in Fig. 10.

The highest energy points in the Ar and Ca plots suggest that the abundance of these two elements, relative to Fe, increase significantly for energies above ~200 GeV per amu. These apparent increases could be due to (*a*) a real increase in the primary abundance ratios Ar/Fe and Ca/Fe, (*b*) a flattening or upturn in the secondary/primary abundances above ~200 GeV per amu, or (*c*) an instrumental artifact associated with the lack of a calibration of the relativistic rise.

One possible instrumental effect which could account for the apparent turnup in the Ar and Ca abundances would be the following: if the ρ versus energy calibration curve for elements lighter than Fe did not flatten off at the highest energies quite as much as does the curve for Fe, then at these highest energies we would be plotting the ratio of Ca at some energy to Fe at a *higher* energy. Because of the steepness of the energy spectra and the flatness of the ρ versus energy curve at these highest energies, only a small difference between Ca (or Ar) and Fe in the value of ρ at a given energy is necessary to change the ratio by a factor of 2. For example, if Ca at $\rho = 1.17$ had the same energy as Fe at $\rho = 1.16$, the two highest energy points on the Ca/Fe plot would fall on the solid line. So if the curve of ρ versus energy for Fe flattens off at high energy a bit quicker than does the curve for Ca, the sharp increase in Ca/Fe at 500 GeV per amu would disappear.

We do not believe that these problems affect our results at energies below ~150 GeV per amu, because at these energies the different elements show different energy dependences (flat for Ni/Fe, power-law fall for secondaries/Fe) in a way that is not surprising. If in our data above 150 GeV per amu the K and Sc abundances would continue to fall while the Ni remained flat and the Ar and Ca turned up, we would be much more confident of the reality of this turnup; however, for none of the secondary elements is there sufficient abundance at these high energies to make any statement.

If future studies demonstrate that our calibration is correct above 150 GeV per amu then the turnup in the data would imply a real effect in the cosmic rays. Because we have no data for the pure secondary elements above ~150 GeV per amu, we cannot exclude the possibility of a flattening or turnup of the secondary/primary ratio at these higher energies. Indeed, such an effect is predicted by the closed-galaxy model of Peters and Westergaard (1977).

If the turnup is due neither to an instrumental artifact nor to a change in the slope of the secondary/primary ratio, then we would have evidence of a difference between the cosmic-ray source composition at several hundred GeV per amu and that at lower energies. Evidence for such a heterogeneity of cosmic-ray sources would be important.

V. CONCLUSIONS

We have shown that the primary elements Ni and Fe have nearly constant relative abundances over the interval 10 to ~500 GeV per amu. While this result implies an energy-independent source composition over this energy interval, it appears that the Ni/Fe ratio at these high energies is appreciably larger than that at ~1 GeV per amu.

We have demonstrated that individual secondary elements which are derived principally from interactions of primary Fe nuclei, display a power-law decrease in relative abundance up to ~150 GeV per amu, in a similar manner to that previously

© American Astronomical Society • Provided by the NASA Astrophysics Data System

1988ApJ...324.1106B

demonstrated for secondary elements from lighter nuclei and for the group of iron secondaries.

The elements Ar and Ca have very substantial secondary components at low energies; at 1 GeV per amu ~80% of the incident Ar and 60% of the incident Ca is secondary. Since the primary and secondary components have different energy dependences, and the secondary fraction decreases with increasing energy, abundance measurements over a wide energy interval permit the determination of the primary component, without use of a galactic propagation to subtract the secondary component. Combining our measurements from 10 to 150 GeV per amu with those of the Danish-French instrument on the same spacecraft between 1 and 25 GeV per amu gives the energy dependence of these abundances over more than two decades of energy. The primary abundances derived from these measurements agree with the Ar/Fe and Ca/Fe ratios previously inferred from lower energy data and confirm a fractionation of source abundances in which elements with high values of the first ionization potential are depleted relative to those with low first ionization potential.

This work was supported in part by NASA grants NAG 8-498, 500, 502, and NGR 05-002-160, 24-005-050, and 26-008-001. R. Cowsik provided helpful comments on the distributed acceleration process. We are grateful to M. A. Olevitch for significant computer systems and programming assistance and to S. D. Barthelmy for discussion of relativistic rise measurements.

REFERENCES

Allison, W. W. M., and Cobb, J. H. 1980, *Ann. Rev. Nucl. Part. Sci.*, **30**, 253.
Anders, E., and Ebihara, M. 1982, *Geochim. Cosmochim Acta*, **46**, 2362.
Awaya, T. 1979, *Nucl. Instr. Meth.*, **165**, 317.
Baker, S., and Cousins, R. D. 1984, *Nucl. Instr. Meth.*, **221**, 437.
Balasubrahmanyan, V. K., and Ormes, J. F. 1973, *Ap. J.*, **186**, 109.
Barthelmy, S. D. 1985, Ph.D. thesis, Washington University, St Louis.
Barthelmy, S. D., Israel, M. H., and Klarmann, J. 1985, *Proc. 19th Internat. Cosmic Ray Conf.* (La Jolla), **2**, 24.
Binns, W. R., Fixsen, D. J., Garrard, T. L., Israel, M. H., Klarmann, J., Stone, E. C., and Waddington, C. J. 1984, *Adv. Space Res.*, **4**, 25.
Binns, W. R., Israel, M. H., Klarmann, J., Scarlett, W. R., Stone, E. C., and Waddington, C. J. 1981, *Nucl. Instr. Meth.*, **185**, 415.
Breneman, H. H., and Stone, E. C. 1985, *Ap. J. (Letters)*, **299**, L57.
Brewster, N. R., Freier, P. S., and Waddington, C. J. 1985, *Ap. J.*, **294**, 419.
Cobb, J. H., Allison, W. W. M., and Bunch, J. N. 1976, *Nucl. Instr. Meth.*, **133**, 315.
Cowsik, R. 1980, *Ap. J.*, **241**, 1195.
———. 1986, *Astr. Ap.*, **155**, 344.
Eichler, D. 1980, *Ap. J.*, **237**, 809.
Engelmann, J. J., *et al.* 1983, *Proc. 18th Internat. Cosmic Ray Conf.* (Bangalore), **2**, 17.
Fransson, C., and Epstein, R. I. 1980, *Ap. J.*, **242**, 411.
Israel, M. H., Jones, M. D., Klarmann, J., Binns, W. R., Garrard, T. L., Stone, E. C., Fickle, R. K., and Waddington, C. J. 1983, *Proc. 18th Internat. Cosmic Ray Conf.* (Bangalore), **9**, 123.
Jones, M. D. 1985, Ph.D. thesis, Washington University, St Louis.
Jones, M. D., Klarmann, J., Stone, E. C., Waddington, J., Binns, W. R., Garrard, T. L., and Israel, M. H. 1985, *Proc. 19th Internat. Cosmic Ray Conf.* (La Jolla), **2**, 28.
Juliusson, E., Meyer, P., and Muller, D. 1972, *Phys. Rev. Letters*, **29**, 445.
Krombel, K. E., and Wiedenbeck, M. E. 1985, *Proc. 19th Internat. Cosmic Ray Conf.* (La Jolla), **2**, 92.
Lund, N. 1984, *Adv. Space Res.*, **4**, 5.
Peters, B., and Westergaard, N. J. 1977, *Ap. Space Sci.*, **48**, 21.
Simon, M., Spiegelhauer, H., Schmidt, W. K. H., Siohan, F., Ormes, J. F., Balasubrahmanyan, V. K., and Arens, J. F. 1980, *Ap. J.*, **239**, 712.
Smith, L. H., Buffington, A., Smoot, G. F., Alvarez, L. W., and Wahlig, M. A. 1973, *Ap. J.*, **180**, 987.
Wandel, A., Eichler, D., Letaw, R. J., Silberberg, R., and Tsao, C. H. 1987, *Ap. J.*, **316**, 696.
Webber, W. R. 1983, in *Composition and Origin of Cosmic Rays*, ed. M. M. Shapiro (Dordrecht: Reidel), p. 83.
———. 1985, in *Cosmic Ray and High Energy Gamma Ray Experiments for the Space Station Era*, ed. W. V. Jones and J. P. Wefel (Louisiana State University: Baton Rouge), p. 283.
Webber, W. R., and Brautigam, D. A. 1982, *Ap. J.*, **260**, 894.
Webber, W. R., Lezniak, J. A., Kish, J. C., and Damle, S. V. 1973, *Nature Phys. Sci.*, **241**, 96.
Westfall, G. D., Wilson, L. W., Lindstrom, P. J., Crawford, H. J., Greiner, D. E., and Heckman, H. H. 1979, *Phys. Rev. C.*, **19**, 1309.

W. R. Binns, M. H. Israel, M. P. Kamionkowski, and J. Klarmann: Department of Physics and the McDonnell Center for the Space Sciences, Washington University, St Louis, MO 63130

T. L. Garrard and E. C. Stone: 220-47 Downs Laboratory, California Institute of Technology, Pasadena, CA 91125

Michael D. Jones: LASP, Campus Box 392, University of Colorado, Boulder, CO 80309

C. J. Waddington: School of Physics and Astronomy, University of Minnesota, 116 Church St., S.E., Minneapolis, MN 55455

© American Astronomical Society • Provided by the NASA Astrophysics Data System